# ACTIVE AEROELASTIC CONTROL OF VARIABLE CAMBER AIRFOIL IN THE PRESENCE OF STRUCTURAL NON-LINEARITIES

**Flávio D. Marques*, Carlos De Marqui Jr.*, Paulo R. Caixeta Jr.***
*** Engineering School of Sao Carlos, University of Sao Paulo**
**Laboratory of Aeroelasticity**

**Keywords**: *Aeroelasticity, variable camber, smart airfoil, fuzzy control, non-linear aeroelasticity*

## Abstract

*Modern smart materials technologies have led to the idea of aircraft that may actively change their shape to maneuver or to control aeroelastic response. In this context, it is reasonable to consider that nonlinear aeroelastic behavior represents an important issue. If an aircraft structure presents mildly or severe non-linear behavior, the active aeroelastic control by means of changing aircraft shape can represent a great challenge. This work presents an investigation on active control of aeroelastic response using variable camber airfoils. Fuzzy aeroelastic control law modeling, where non-linear structural behavior is considered, has been aimed. Distributed lumped vortex method has been used to determine unsteady aerodynamic responses and typical structural non-linearities have been also adopted for the aeroelastic simulation. Active camber variation is achieved by means of time-varying polynomial description of the airfoil camber line. The results show a robust and acceptable methodology to threat aeroelastic response control of variable shape aerodynamic structures.*

## 1 Introduction

Generally aircrafts are optimised for specific flight conditions. When an aircraft operates away from these optimal design points, the performance can decline. Nowadays the interest in air vehicles that can operate in several conditions, such as efficiency in subsonic and supersonic cruise or high manoeuvrability is increasing. The use of adaptive technologies can be a solution to improve the performance at conflicting conditions and increase the optimum flight envelope [1]. Lifting surfaces with variable geometry can be one of these technologies. The recent development of smart materials has been pointed out as an important factor to the development of this kind of structure [2].

Traditionally the geometry of a lifting surface has been modified in many different ways. Maybe, the most usual one is the use of hinged surfaces, such as flaps and trim tabs, to modify the camber. Some other usual form of geometry modification can be wing warping, wing sweep, wing twist [3]. These traditional forms of modifications are limited by the aerodynamic and structural requirements of an aircraft and are efficient in a specific range of velocities, for example. The development of lifting surfaces that can change their geometry actively and smoothly through the camber variation, twist angle and sweep angle variation can eliminate the need for the conventional forms of geometry modification [4][5][6]. This new technology can increase the aerodynamic and aeroelastic performance of lifting surfaces in a wide range of conditions through the active flow control and active control of aeroelastic responses. These benefits will imply in a more efficient structural design.

The smooth variation of camber has been studied by many authors and is the main interest

of this work. In the 1970s the Mission Adaptive Wing program demonstrated on the F-111 a smooth camber variation in chordwise direction [7]. The Active Aeroelastic Wing utilizes multiple leading-edge and trailing-edge control surfaces to use possible benefits of wing twist [8]. The development of a flexible flap to be used in a civil transport aircraft that allows smooth camber variations is described in [9] and [10]. The aerodynamic, aeroelastic and structural benefits are clearly shown by these authors.

Some other authors have studied the application of smart materials to achieve the smooth and active geometry modification. An analytical study of a wing with variable geometry using piezoelectric patches as actuators was developed by [11]. Several improvements in aerodynamic performance and control of static aeroelastic characteristics are observed. A wind tunnel wing model that uses shape memory alloy torque tubes to twist the wing and shape memory alloy wires to smoothly deform trailing-edge control surfaces was developed by [1]. Comparisons between a conventional hinged control surface and the shape memory alloy actuated wing show the aerodynamic and aeroelastic benefits of the new technology. Previously to the experimental tests the aerodynamic and aeroelastic performance were investigated using a computational code that associates a vortex lattice method and finite element modeling. In the same line, a method to study the structural behaviour and static aeroelastic response of a general wing has developed by [12]. The structural model is based on the assumption that the wing behaves like a plate and can be modeled by the first order shear deformation theory and a compressible vortex lattice code is used for aerodynamic model. The manoeuvre, aerodynamic and aeroelastic improvements were demonstrated for a wing that can modify camber and twist angle.

The new structures obtained with these new technologies will certainly have inherent non-linearities, as is already verified in real aircraft structures. Different types of structural and aerodynamic non-linearities are commonly encountered in aeronautical engineering. A comprehensive study of some different types of non-linearities present on aeroelastic systems can be found in [13]. Non-linear aerodynamic effects are more difficult to analyse since the fluid motion is governed by equations where analytical solutions are practically non-existent. Structural non-linearities arise from worn hinges of control surfaces, loose control linkages, material behaviour and various other sources. Aging aircraft and combat aircraft that carry heavy external stores are more likely to be influenced by effects associated with non-linear structures. This type of non-linearity can be treated as a concentrated non-linearity, and usually can be approximated by one of the classical structural non-linearities, namely, cubic, free-play and hysteresis.

The consequences of the non-linear aeroelastic responses and their control have been widely studied. Fighter aircrafts have experienced limit cycle oscillations for some attached wing store configurations. The mechanism that leads to these LCOs is not well understood, but explanations have included aerodynamic and/or structural non-linearities [14]. Stiffness tests show evidences of a spring-hardening non-linearity in the wing torsional mode. This type of non-linearity will lead to LCO behavior similar to the described in one of the non-linearities verified in this work. Several authors have developed control strategies for non-linear aeroelastic phenomena suppression [14][15][16][17].

This paper presents the study of non-linear aeroelastic behaviour of an airfoil. The non-linear aeroelastic response is then suppressed by means of variable geometry lifting surface, more specifically variation of camber in chordwise direction. The non-linear structural behaviour is obtained assuming non-linear stiffening in pitching, represented by a cubic polynomial and a free-play. An aeroelastic model is accomplished using unsteady lumped vortex method. A fuzzy logic controller emulated with a neural network is used as a preliminary tool in order to test the control actuation concept.

## 2 Aeroelastic Model

A two-dimensional airfoil having two degree of freedom, as depicted in Fig. 1, is investigated.

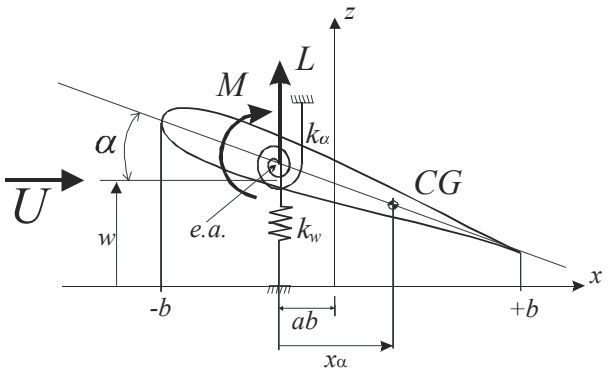


**Fig. 1.** Structural representation of the aeroelastic model.

The bending and torsional variables are denoted as $w$ and $\alpha$, respectively, and the equations of motion for this typical section are obtained as in [18],

$$\begin{bmatrix} m & -mx_\alpha b \\ -mx_\alpha b & I_\alpha \end{bmatrix} \begin{Bmatrix} \ddot{w} \\ \ddot{\alpha} \end{Bmatrix} + \begin{bmatrix} k_w & 0 \\ 0 & k_\alpha(\alpha) \end{bmatrix} \begin{Bmatrix} w \\ \alpha \end{Bmatrix} = \begin{Bmatrix} L \\ M \end{Bmatrix} \quad (1)$$

In Eq. (1), $m$ the mass of the system; $I_\alpha$ is the mass moment of inertia about the elastic axis; $x_\alpha$ is the non-dimensionalized distance between the centre of mass and elastic axis; $L$ and $M$ are the aerodynamic lift and moment; $b$ is the semichord of the wing and the two structural spring forces are represented by $k_w$ and $k_\alpha$ for bending and torsion, respectively.

Non-linear effects due to aerodynamics, damping or structural dynamics can be incorporated to this model. In this work, the structural damping effects are neglected and the source of non-linearities is assumed to be the non-linear torsion spring, which will result in the non-linear moment. The polynomial form of Eq. (2) can be an approximation of this kind of non-linearity [17]. This is shown in Fig. 2 (a), where $f(\alpha)=k_\alpha\alpha$ is the non-linear structural moment.

$$k_\alpha(\alpha) = k_{\alpha_0} + k_{\alpha_1}\alpha + k_{\alpha_2}\alpha^2 + k_{\alpha_3}\alpha^3 \cdots \quad (2)$$

Another form of non-linearity that can be assumed for the pitching stiffness is the free-play one [19]. This kind of non-linearity is represented mathematically by Eq. (3) and the non-linear structural moment is shown in Fig. 2 (b).

$$\begin{aligned} f(\alpha) &= k_\alpha(\alpha - \alpha_f), && \alpha > +\alpha_f \\ f(\alpha) &= 0, && -\alpha_f \le \alpha \le +\alpha_f \\ f(\alpha) &= k_\alpha(\alpha + \alpha_f), && \alpha < -\alpha_f \end{aligned} \quad (3)$$

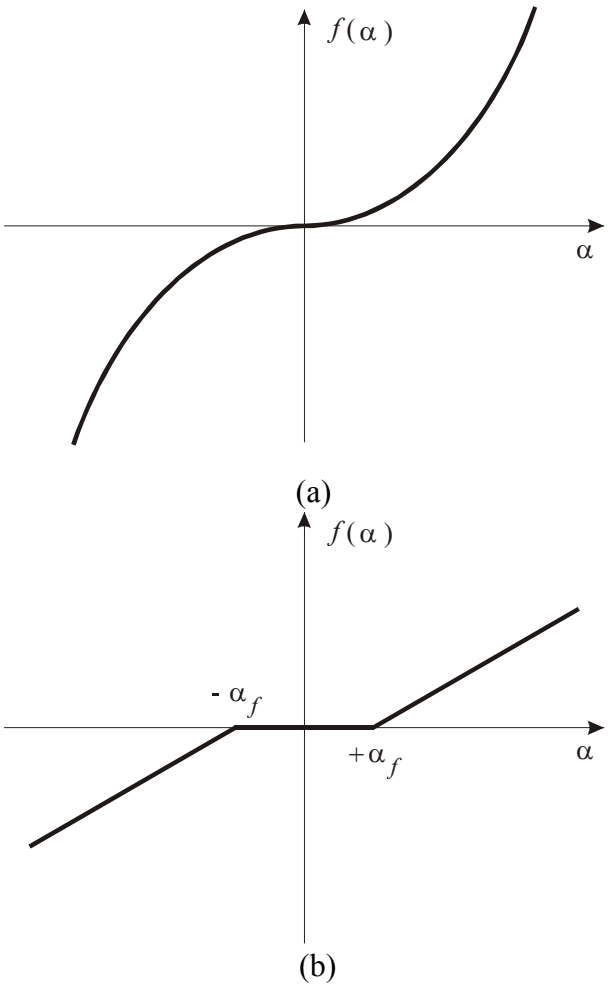


**Fig. 2.** Non-linear pitch stiffness: (a) Polynomial non-linearity; (b) Free-play non-linearity.

An aerodynamic model has to be assumed to represent the terms on the right side of Eq. (1). The solution of an aeroelastic problem is strictly connected to the quality of the aerodynamic model. The unsteady air load over the airfoil for the incompressible potential flow is solved with the lumped vortex method [20]. The applied numerical method was modified to make possible the time variation in airfoil camber. The method seems to be appropriate for the calculation of the air load on the airfoil with variable geometry, but it is computationally more demanding if compared with that for the rigid airfoil case. Within every time step a new position of point vortices and collocation points must be evaluated.

The airfoil is described by a set of discrete vortices on the camberline, $\Gamma_j$, as observed in Fig. 3. When the airfoil's circulation changes, the vortex wake elements, $\Gamma_W$, are shed at the trailing edge and the wake is modeled using the same vortex element. Two boundary conditions are defined: the zero normal velocity across de body's solid boundaries and the flow disturbance, due to body motion through the fluid, should diminish far away from the body. Also, Kelvin condition and Kutta theorem have to be respected.

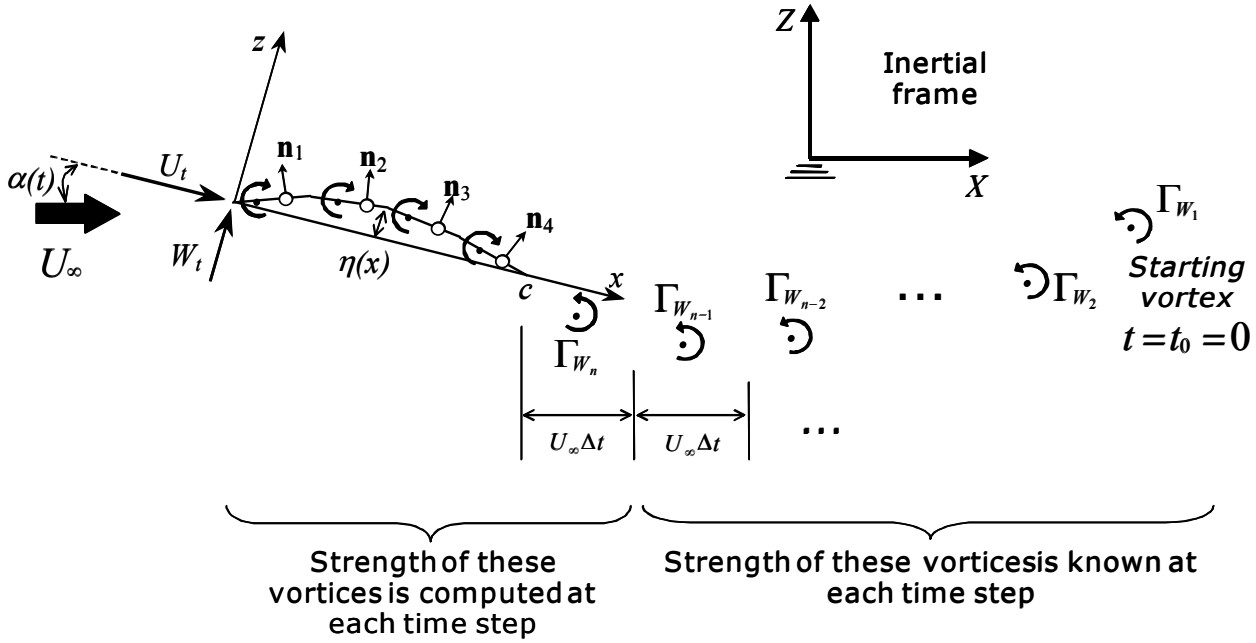


**Fig. 3**. Discrete vortex model for the unsteady air load on the airfoil calculation [20].

The induced velocities, $u$ and $w$, at an arbitrary point $(x, z)$ due to a vortex element $\Gamma_j$ located at $(x_j, z_j)$ is given by Eq. (4), where $r_j^2 = (x - x_j)^2 + (z - z_j)^2$.

$$\begin{Bmatrix} u \\ w \end{Bmatrix} = \frac{\Gamma_j}{2\pi\, r_j^2} \begin{bmatrix} 0 & 1 \\ -1 & 0 \end{bmatrix} \begin{Bmatrix} x - x_j \\ z - z_j \end{Bmatrix} \qquad (4)$$

Considering that the airfoil camberline is divided into $N$ panels, the vortex points $(x_j, z_j)$ are placed at the quarter chord of each planar panel and the zero normal flow boundary condition can be fulfilled on the camberline at the three quarter point (collocation point) of each panel. The normal vector $\boldsymbol{n}_i$ at each of these collocation points is found in the body's frame from the surface shape $\eta(x)$ is,

$$\mathbf{n}_i = \frac{(-d\eta/dx, 1)}{\sqrt{(d\eta/dx)^2 + 1}} = (sin\alpha_i, \cos\alpha_i) \qquad (5)$$

As the airfoil's geometry changes with time in the case considered by this paper, vortex

and collocation points calculations have to be done at each time step loop.

The influence coefficient $a_{ij}$ is defined as the velocity component induced by the airfoil's unit strength $\Gamma_j$ element, normal to the surface at the collocation point $i$. The set of algebraic equations shown in Eq. (6) are obtained for each collocation point. In Eq. (6), the right-hand side (*RHS*) terms are known at each time steps and are composed by the kinematic velocities due to the motion of the airfoil plus the velocity components induced by wake vortices, except the latest one. As the airfoil's geometry changes with time, the influence coefficient calculation has to be done at each time step loop.

$$\begin{bmatrix} a_{11} & a_{12} & \cdots & a_{1N} & a_{1W} \\ a_{21} & a_{22} & \cdots & a_{2N} & a_{2W} \\ \vdots & \vdots & \ddots & \vdots & \vdots \\ a_{N1} & a_{N2} & \cdots & a_{NN} & a_{NW} \\ 1 & 1 & \cdots & 1 & 1 \end{bmatrix} \begin{Bmatrix} \Gamma_1 \\ \Gamma_2 \\ \vdots \\ \Gamma_N \\ \Gamma_{W_t} \end{Bmatrix} = \begin{Bmatrix} RHS_1 \\ RHS_2 \\ \vdots \\ RHS_N \\ \Gamma(t-\Delta t) \end{Bmatrix} \quad (6)$$

The Kutta condition is not stated explicitly for the lumped vortex method and the Kelvin condition is represented by Eq. (7).

$$\Gamma(t) - \Gamma(t-\Delta t) + \Gamma_W = 0 \quad (7)$$

Subsequently, the pressures and loads are computed by using the unsteady Bernoulli equation. The total lift and moment are obtained by integrating the pressure difference between the camberline upper and lower surfaces along the chordline. At this point, all the terms necessary to the solution of Eq. (1) are known and it can be solved with the Runge-Kutta method, for example.

## 3 Deformable camber and control law

Airfoils with variations in geometry can be applied in two main categories. The first one can be described as small and slow alterations of airfoil's geometry that makes possible the optimisation of shape according to the flight conditions. In the second one, faster and major changes will damp vibrations and aeroelastic phenomena, for example [11][10]. In this work, an airfoil with camber variation is used to damp non-linear aeroelastic responses. The actuators necessary to change the airfoil's camber are considered ideal.

The original, or non-deformed airfoil, is a symmetric one and its straight camber line is represented in Fig. 4. The variation in airfoil's camber is approximated by a third-order polynomial shown in Eq. (8), where *G(t)* is a gain that modifies the amplitude of the camber at each time step. An example of camber variation approximated by a third-order polynomial is shown in Fig. 4.

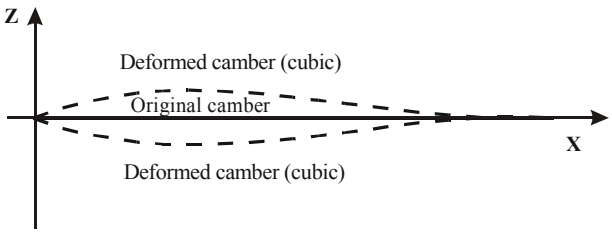


**Fig. 4.** Representation of the original mean camber line and the deformed camber line represented by a third-order polynomial.

$$camber(x,t) = (A_0 x^0 + A_1 x^1 + A_2 x^2 + A_3 x^3) \times G(t) \quad (8)$$

In order to suppress aeroelastic responses, linear or non-linear, a controller has to be designed. A fuzzy logic controller based on the Mamdani-type fuzzy model is applied. Membership functions and a set of rules are defined based on the previous experience obtained from simulations performed with the non-linear aeroelastic model and a decision surface is obtained. The decision surface represents, therefore, the control law on a unitary discourse universe. The control law models the consequent control action like a PD-type controller.

When PD fuzzy controllers are considered the controller inputs are defined as an error and the variation of this error. The error is the difference between the feedback variable and a reference value. The torsional and bending displacements, $\alpha$ and $w$ of Eq. (1), are used to calculate the controller input signals. The error defined in this work is a composed one, as is observed in Eq. (9). It is the summation of the bending error and the torsional error. The torsional error is the difference between the

torsional angle and the zero value and the bending error is the difference between the bending displacement and the zero value. The importance of the bending error and the torsional error to the value of the composed error is quantified by the values of the weights $W_\alpha$ and $W_w$. The gain that modify the camber amplitude $G(t)$ is the output of the controller and will change the airfoil's shape.

$$Error(t) = W_\alpha(ref - \alpha(t)) + W_w(ref - w(t)) \qquad (9)$$

The input and output signals are normalized by individual gains. These gains are obtained manually and they guarantee stable and efficient response control. The fuzzy membership functions are also obtained and tuned manually. Table 1 shows the rule basis and Fig. 5 the respective decision surface, where $Z$ is zero, $+S$ is negative small, $-M$ is negative medium, $-L$ is negative large, $+S$ is positive small, $+M$ is positive medium, $+L$ is positive large.

**Table 1.** Rule basis of the fuzzy controller.

| | | Variation of error | | | | | | |
|---|---|---|---|---|---|---|---|---|
| | | -L | -M | -L | Z | +S | +M | +L |
| Error | -L | -L | -L | -L | -L | -M | -S | Z |
| | -M | -L | -L | -M | -M | -S | Z | +S |
| | -S | -L | -M | -S | -S | Z | +S | +M |
| | Z | -L | -M | -S | Z | +S | +M | +L |
| | +S | -M | -S | Z | +S | +S | +M | +L |
| | +M | -S | Z | +S | +M | +M | +L | +L |
| | +L | Z | +S | +M | +L | +L | +L | +L |

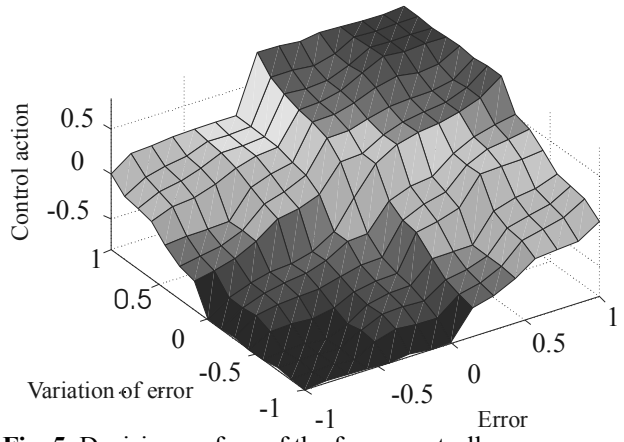


**Fig. 5**. Decision surface of the fuzzy controller.

## 4 Aeroelastic response control and LCO avoidance

### 4.1 Linear analysis

This subsection presents a study on aeroelastic linear problem of the two-dimensional airfoil section. The set of dimensionless parameters are taken as those in [18] and shown in Tab. 2.

**Table 2.** System parameters obtained from [18], pp. 219.

| | |
|---|---|
| b = 0.127 m | $\omega_\alpha$ = 64.1 rad/s |
| a = - 0.15 | $\omega_w$ = 55.9 rad/s |
| $\mu$ = 76 | $x_\alpha$ = 0.25 |
| $r_\alpha^2$ = 0.388 | $\rho$ = 1.225 kg/m$^3$ |

In Tab. 1 the dimensionless parameters are defined as

$$r_\alpha^2 = \frac{I_\alpha}{mb^2}, \quad x_\alpha = \frac{S_\alpha}{mb}, \quad \omega_w^2 = \frac{k_w}{m}, \quad \omega_\alpha^2 = \frac{k_\alpha}{I_\alpha},$$
$$m = \mu\pi\rho b^2$$

where $\omega_w$ and $\omega_\alpha$ are the bending and torsional frequencies; $r_\alpha$ is the radius of gyration; $\mu$ is the mass ratio; $S_\alpha$ is the static moment; $a$ is non-dimensionalized distance from the midchord to the elastic axis.

Critical flutter speed of 27.5 *m/s* and flutter frequency of 9.5 Hz are determined solving the flutter determinant with Theodorsen's function been considered for unsteady aerodynamics [18]. This critical speed is calculated neglecting the effects of structural damping. The aeroelastic model shown in Eq. (1) also neglects the effect of structural damping.

The critical flutter speed obtained with the aeroelastic model described in Section 1 (considering 20 panels) is 26.0 *m/s* and the flutter frequency is 8.4 Hz, what is close to Fung's results. The open-loop linear aeroelastic responses for bending and torsional displacements at critical flutter speed are shown in Fig. 6 and 7, respectively. The results obtained in Fig. 6 could validate the aeroelastic model developed in this work.

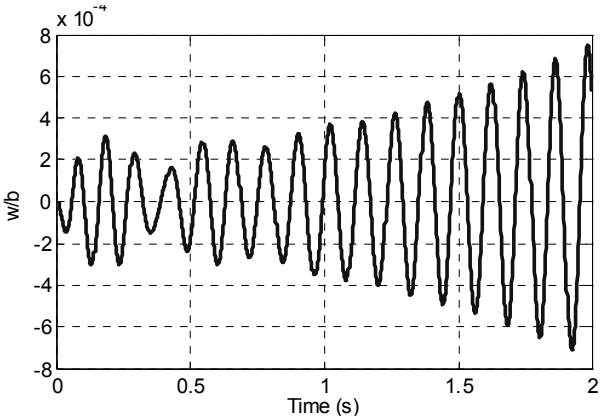


**Fig. 6.** Open-loop linear aeroelastic response for bending displacement.

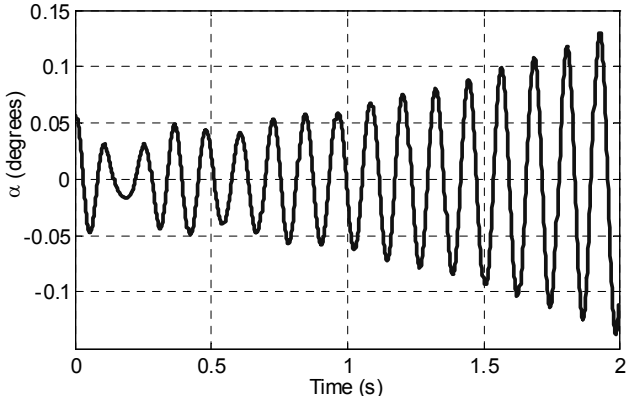


**Fig. 7.** Open-loop linear aeroelastic response for torsional displacement.

### 4.2 Non-linear analysis and control

This subsection presents the analysis of non-linear aeroelastic response of the two-dimensional airfoil section. The source of non-linearities is assumed to be the non-linear torsion spring. The non-linear structural behaviour is obtained assuming the non-linear moment $f(\alpha)$ represented by a cubic polynomial and free-play.

The cubic polynomial used to represent the non-linear moment during the simulations is shown in Eq. (10). This equation was obtained from a curve fitting performed with some points chosen near linear moment curve with respect to the angle of attack.

$$f(\alpha) = 6000\alpha^3 + 0.49\alpha \qquad (10)$$

To verify the non-linear aeroelastic behavior and the performance of the Fuzzy controller the numerical simulations are performed with a freestream velocity of 31.5 *m/s*, that exceeds the linear critical flutter velocity ($U_{cr} \cong 26$ *m/s*). The parameters shown in Tab. 1 are retained. The open-loop non-linear responses with the initial conditions $w = 0.015$ *m* and $\alpha = 0.3$ *degrees* are shown in Fig. 8 and 9. Figure 10 and 11 show the phase trajectories for open-loop bending and torsional responses. The limit cycle oscillations behaviour is observed in these responses.

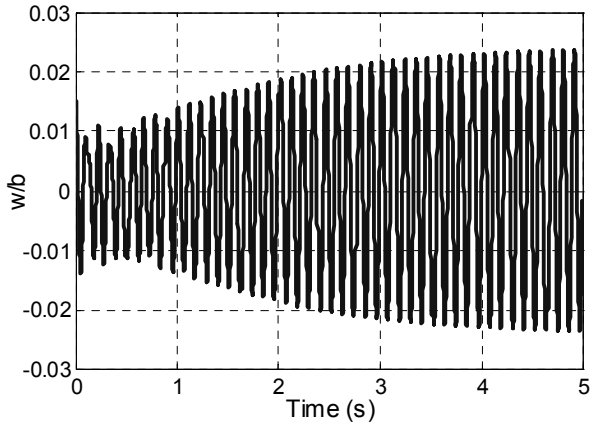


**Fig. 8.** Non-linear open-loop bending response (U = 31.5 *m/s*).

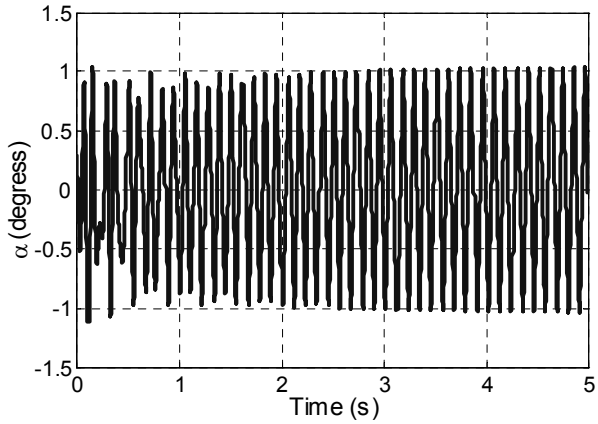


**Fig. 9.** Non-linear open-loop torsional response (U = 31.5 *m/s*).

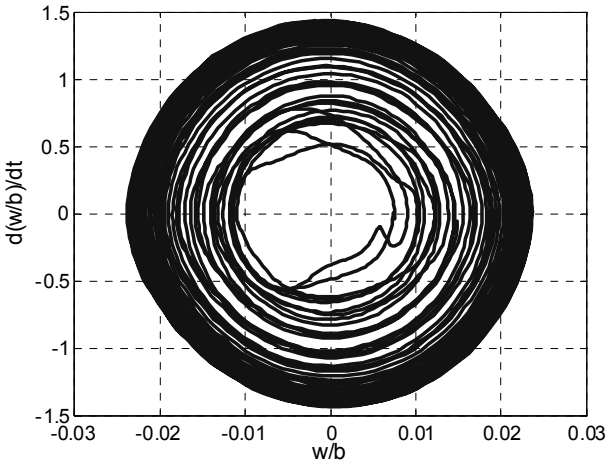


**Fig. 10.** Phase trajectory of bending response.

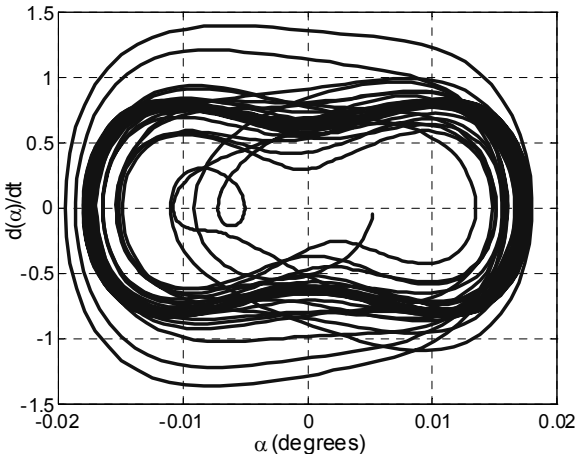


**Fig. 11.** Phase trajectory of torsional response.

The parameters of the third-order polynomial, Eq. (8), that approximate the airfoil's camber variation are set to $A_0 = 0$, $A_1 = 0.875$, $A_2 = 1.875$ and $A_3 = 1$. The controller gains used to normalize the input and output signals of the fuzzy controller are set to $Gain_{\text{error}} = 10^{-3}$, $Gain_{\text{Verror}} = 10^{-4}$ and $Gain_{co} = 0.35$. Figure 8 shows the closed-loop bending and torsional responses. The loop is closed at time 3.0 seconds.

The closed loop bending and torsional responses in Fig. 12 and 13 converge to zero. The settling time for stabilization of non-linear bending and torsional responses is of the order of 1.2 seconds.

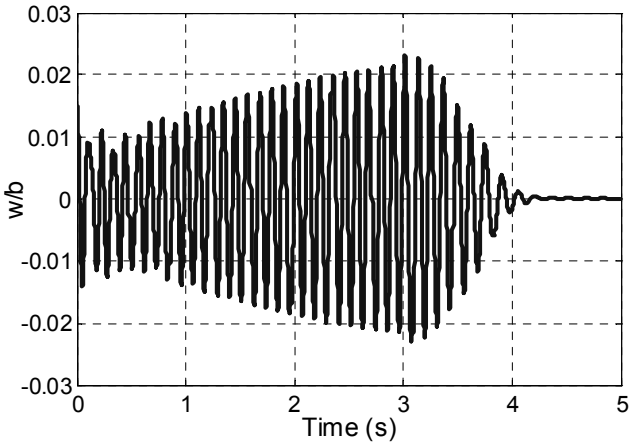


**Fig. 12.** Closed-loop bending response.

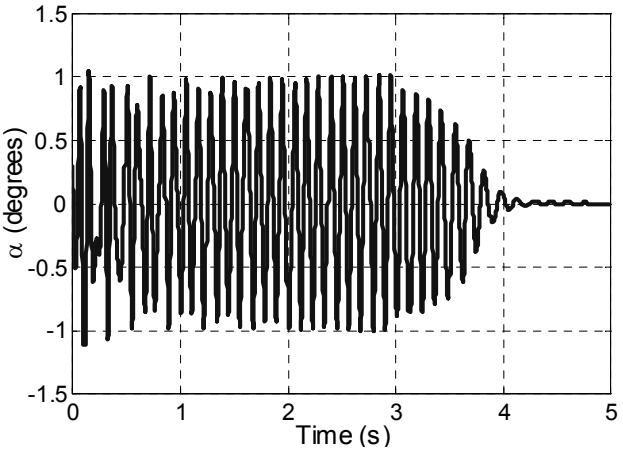


**Fig. 13.** Closed-loop torsional response.

Figure 14 shows the airfoil's camber variations during the suppression of the LCO behaviour. Figure 14(a) shows the camber variation during the entire LCO control simulation. Figure 14(b) shows a detailed view of the region where the largest camber amplitudes (± 2% of the chord) were necessary for control action, between 3.0 to 4.2 seconds.

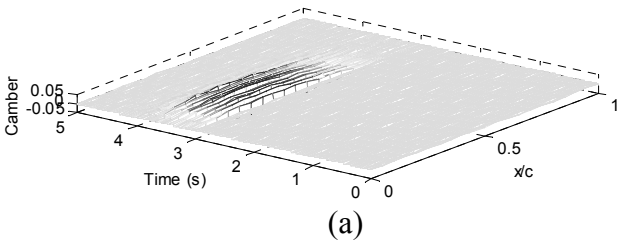


(a)

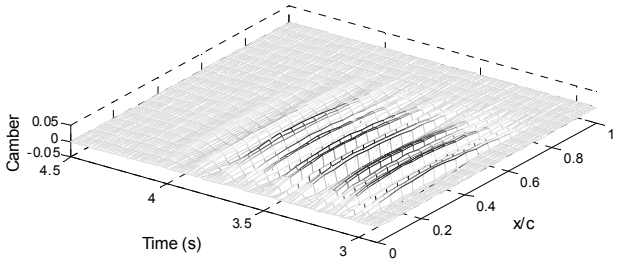


(b)

**Fig. 14.** Variation of camber line during the closed-loop simulations.

The free-play is the second source of non-linearity verified during the simulations. The free-play magnitude $\alpha_f$ is taken to be 0.5°, as can be observed in Eq. (11).

$$\begin{aligned} f(\alpha) &= k_\alpha(\alpha - 0.5), \qquad \alpha > 0.5 \\ f(\alpha) &= 0, \qquad -0.5 \le \alpha \le +0.5 \\ f(\alpha) &= k_\alpha(\alpha + 0.5), \qquad \alpha < -0.5 \end{aligned} \tag{11}$$

To verify the non-linear aeroelastic behavior and the performance of the Fuzzy controller the numerical simulations are performed with a freestream velocity of 31.5 *m/s*, that exceeds the linear critical flutter velocity ($U_{cr} \cong 26$ *m/s*). The parameters shown in Tab. 1 are retained. The open-loop non-linear responses with the initial conditions $w$ = 0.0 *m* and $\alpha$ = 0.5 *degrees* are shown in Fig. 15 and 16. Figure 17 and 18 show the phase trajectories for open-loop bending and torsional responses. As can be verified, the non-linear aeroelastic system has two equilibrium points.

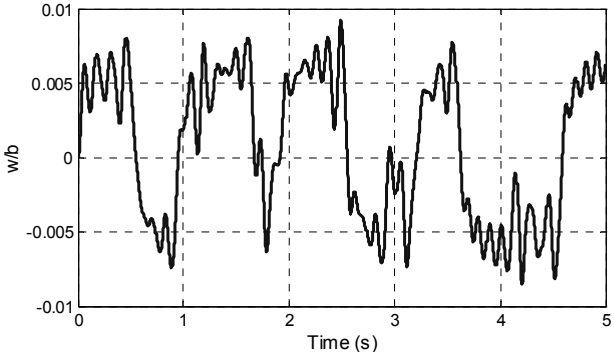


**Fig. 15.** Non-linear open-loop bending response (U = 31.5 *m/s*).

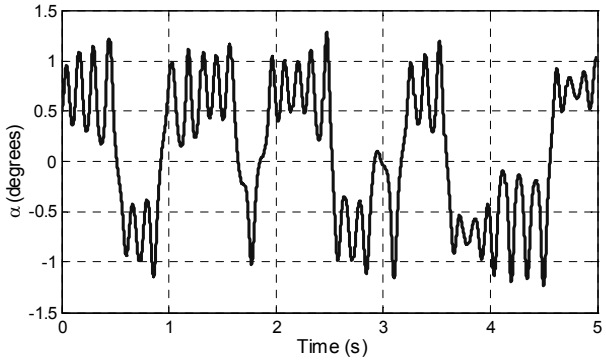


**Fig. 16.** Non-linear open-loop torsional response (U = 31.5 *m/s*).

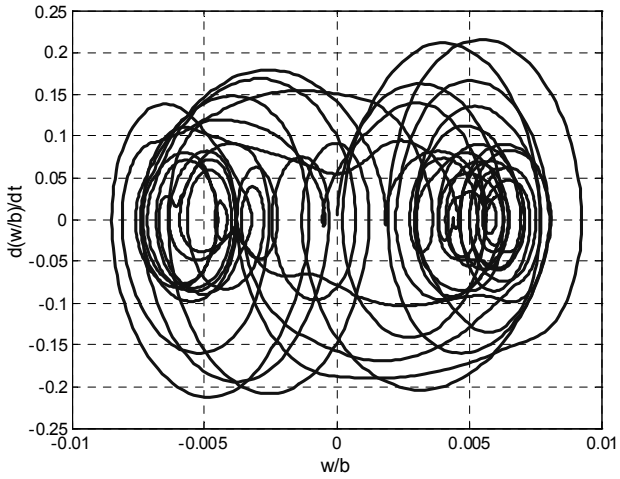


**Fig. 17.** Phase trajectory of bending response.

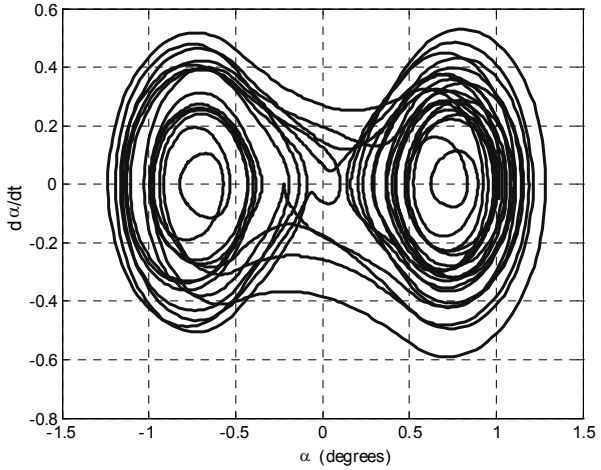


**Fig. 18.** Phase trajectory of torsional response.

The controller gains used to normalize the input and output signals of the fuzzy controller are set to $Gain_{\text{error}} = 10^{-3}$, $Gain_{\text{Verror}} = 10^{-4}$ and $Gain_{co} = 0.35$. Figures 19 and 20 show the

closed-loop bending and torsional responses. The loop is closed at time 3.0 seconds.

The closed loop bending and torsional responses in Fig. 19 and 20 converge to zero. The settling time for stabilization of non-linear bending and torsional responses for the free-play case is very low.

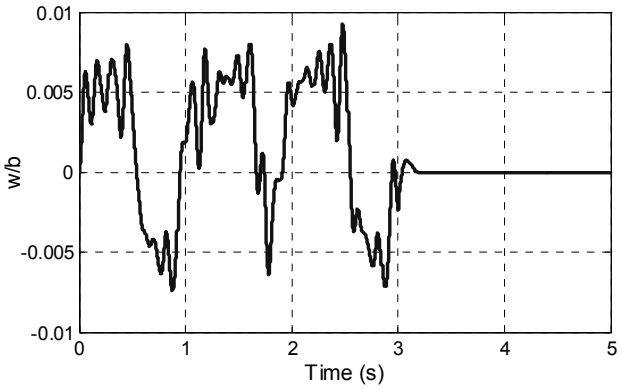


**Fig. 19.** Closed-loop bending response.

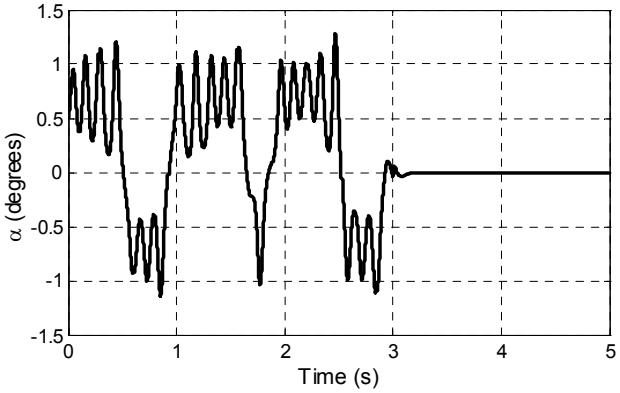


**Fig. 20.** Closed-loop torsional response.

Figure 21 shows the airfoil's camber variations during the suppression of the non-linear response. Figure 21(a) shows the camber variation during the entire control simulation. Figure 21(b) shows a detailed view of the region where the largest camber amplitudes (± 2% of the chord) were necessary for control action, between 3.0 to 3.5 seconds.

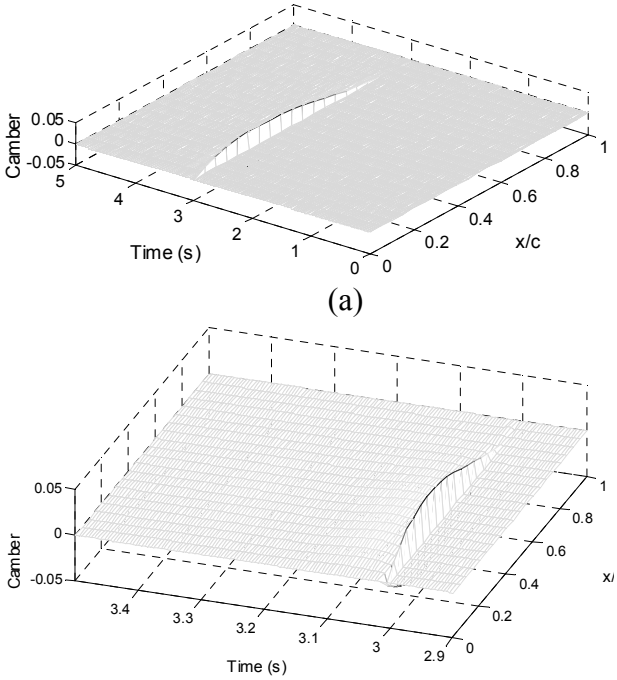


**Fig. 21.** Variation of camber line during the closed-loop simulations.

## 5 Conclusions

An aeroelastic model was used to study the non-linear aeroelastic responses and their control by means of active variable camber. The unsteady aerodynamics was modeled with a lumped vortex method. For the linear analysis a good agreement with results presented in technical literature [18] was shown. Linear behaviour was investigated to provide a reference to the inclusion of non-linear effects. Polynomial and free-play non-linearities were used to describe concentrated torsional moment for the aeroelastic modeling.

The use of a lifting surface (2D) with variable camber can be considered an important alternative for future developments of adaptive aircrafts. This kind of actuation associated with the designed fuzzy controller has shown to be a good combination in the suppression of non-linear aeroelastic responses, in particular to limit cycle oscillations avoidance. The time-varying polynomial description of the airfoil camber line has a great influence in the performance of the controller. During the simulations some different polynomials were tested. It is clear that an optimised one exists and a more detailed investigation is necessary.

Ideal actuators were considered in this initial investigation. Figures 14 and 21 show that small amplitudes in camber were enough to control the non-linear responses. The results achieved in the control of non-linear aeroelastic responses through the camber variation show that future investigations considering the actuation with of smart materials are pertinent.

## 6 References

[1] Sanders, B, Eastep, FE and Forster, B. Aerodynamic and Aeroelastic Characteristics of Wings with Conformal Control Surfaces for Morphing Wings. *Journal of Aircraft*, Vol. 40, No. 1, pp. 94-99, 2003.

[2] Johnston, CO. *Actuator-Work Concepts Applied to Morphing and Conventional Aerodynamic Control Devices*. Thesis – Virginia Polytechnic Institute and State University, Blacksburg, 2003.

[3] Bowman, J, Sanders, B and Weishaar, T. Evaluating the Impact of Morphing Technologies on Aircraft Performance. *AIAA Paper 2002-1631*, 2002.

[4] Pern, NJ and Jacob, JD. Aerodynamic Flow Control Using Shape Adaptive Surfaces. *Proceedings of 1999 ASME Design Engineering Technical Conferences*, Las Vegas, Nevada, USA, 1999.

[5] Sanders, B, Crowe, R and Garcia, E. Defense Advanced Research Projects Agency – Smart Materials and Structures Demonstration Program Overview. *Journal of Inteligent Material System and Structures*, Vol. 15, pp. 227-233, 2004.

[6] Simpsom, JO, Wise, SA, Bryant, RG, Cano, RJ, Gates, TS, Hinkley, JA, Rogowski, RS and Whitley, KS. Innovative Materials for Aircraft Morphing. *Proceedings of the SPIE Smart Structures and Materials Symposium, Industrial and Commercial Applications Conference,* Vol. 3326, Paper 3326-26, 1998.

[7] Smith, S B and Nelson, D W. Determination of the Aerodynamic Characteristics of the Mission Adaptive Wing. *Journal of Aircraft*, Vol. 27, pp. 950-958, 1990.

[8] Pendleton, E, Bessete, D, Field, P, Miller, G and Griffin, K. Active Aeroelastic Wing Flight Research Program: Technical Program and Model Analytical Development. *Journal of Aircraft*, Vol.37, No. 4, pp. 554-561, 2000.

[9] Monner, HP. Realization of na optimized wing camber by using formvariable flap structures. *Aerospace Science and Technology*, Vol. 5, pp. 445-455, 2001.

[10] Stanewsky, E. Aerodynamic benefits of adaptive wing technology. *Aerospace Science and Technology*, Vol. 4, pp. 439-452, 2000.

[11] Ehlers, SM and Weisshaar, TA. Static aeroelastic control of an adaptive lifting surface. *Journal of Aircraft*, Vol. 30, No. 4, pp. 534-540, 1993.

[12] Gern, FH., Inman, DJ and Kapania, RK. Structural and Aeroelastic Modeling of General Planform Wings with Morphing Airfoils. *AIAA Journal*, Vol. 40, No. 4, pp. 628-637, 2002.

[13] Lee, BHK, Price, SJ and Wong, WS. Non-linear aeroelastic analysis of airfoils: bifurcation and chaos. *Progress in Aerospace Sciences*, Vol. 35, pp. 205-334, 1999.

[14] Block, JJ and Strganac, TW. Applied active control for a nonlinear aeroelastic structure. *Journal of Guidance, Control and Dynamics*, Vol.21, No.6. 1998.

[15] Singh, SN and Yim, W. State feedback control of an aeroelastic system with structural nonlinearity. *Aerospace Science and Technology*, No. 7, pp. 23-31, 2003.

[16] Zhang R and Singh SN. Adaptive output feedback control of an aeroelastic system with unstructured uncertainties. *Journal of Guidance, Control, and Dynamics*, Vol.24, No. 3, pp. 502–509, 2001.

[17] Ko, J, Kurdila, A J and Strganac, TJ. Adaptive Feedback Linearization for the Control of a Typical Wing Section with Structural Nonlinearity. *Proceedings of ASME International Mechanical Engineering Congress and Exposition*, Dallas, Texas, 1997.

[18] Fung, YC. *An Introduction to the theory of aeroelasticity*. John Wiley & Sons Inc, USA, 1993.

[19] Tang, D M and Dowell, E H. Flutter and Stall Response of a Helicopter Blade with Structural Nonlinearity. *Journal of Aircraft*, Vol. 29, No.5, pp. 953-960, 1992.

[20] Katz, J. and Plotkin, A. *Low-speed Aerodynamics*. Cambridge University Press, UK, 2001.